JEMAT 2022, Vol 10, No 2, 48-58
https://doi.org/10.54987/jemat.v10i2.773

HIBISCUS PUBLISHER

JOURNAL OF ENVIRONMENTAL MICROBIOLOGY AND TOXICOLOGY

Website: http://journal.hibiscuspublisher.com/index.php/JEMAT/index

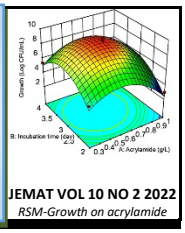

Modelling the Kinetics of Tartrazine Sorption by Bottom Ash

Nur Adeela Yasid[1], Ain Aqilah Basirun[1] and Hartinie Marbawi[2]*

[1]Department of Biochemistry, Faculty of Biotechnology and Biomolecular Sciences, Universiti Putra Malaysia, 43400 UPM Serdang, Selangor, D. E, Malaysia.
[2]Biotechnology Programme, Faculty of Science and Natural Resources, Universiti Malaysia Sabah, 88400 Kota Kinabalu, Sabah, Malaysia.

*Corresponding author:
Hartinie Marbawi
Biotechnology Programme,
Faculty of Science and Natural Resources,
Universiti Malaysia Sabah,
88400 Kota Kinabalu, Sabah,
Malaysia.
Email: hartinie@ums.edu.my

HISTORY

Received: 18th Nov 2022
Received in revised form: 24th Dec 2022
Accepted: 28th Dec 2022

KEYWORDS

Adsorption
Tartrazine
Bottom ash
Kinetics
Error function

ABSTRACT

Bottom ash is the solid residue left over from municipal waste combustion or incineration in a Municipal Waste Incineration Furnace. Its use as a sorption agent, particularly for dye sorption, is a new and important application. Linearized adsorption kinetics has drawbacks such as inaccurate representation of the parameters' 95 percent confidence interval output, unbalanced attention to potential outliers, and magnification of errors may result in inaccurate parameter values. In this study, we used nonlinear regression to investigate 16 adsorption kinetics models of tartrazine by bottom ash. The pseudo-second order was the best model based on the Bias and Accuracy factor near unity, but based on other error function analysis, this model performs equally well with the exponential and fractal-like pseudo-second order based other error functions such as Root-Mean-Square Error (*RMSE*), adjusted coefficient of determination ($adjR^2$), Marquardt's percent standard deviation (MPSD), Bayesian Information Criterion (BIC), Hannan-Quinn Information Criterion (HQC), and especially the corrected Akaike Information Criterion (AICc) function as the absolute difference is 5 absolute unit making discriminatory activity difficult. Furthermore, because the pseudo-second order and exponential models have only two parameters, they are less complicated according to Occam's razor. Because the pseudo-second order model is more popular and has more applications than the less well-known exponential model, we chose it as the best model for tartrazine sorption to bottom ash. Kinetic analysis using the PSO model gave a value of equilibrium adsorption capacity, q_e of 21.88 mg g^{-1} (95% confidence interval (C.I.), 20.93 to 22.84) and k_2 (g/(mg.sec)) of 0.00002 (95%, C.I., 0.00001 to 0.00002).

INTRODUCTION

Every year, around 60,000 tons of dyes are released into the environment as waste, with azo dyes accounting for 80 percent of the total [1–3]. Textile, food, paper, cosmetic, and medical and research industries are all sources of dye pollution [4–7]. Dye pollution is still on the rise in many developing countries with lax regulations on dye manufacturing and use. Malaysia, India, Pakistan, and Bangladesh are examples of these countries [8,9]. In Malaysia, Juru riverine area was documented to have high-level contamination of dye pollution [9,10]. Effluents from dye-using industries are typically discharged directly into bodies of water, posing a significant wastewater treatment concern [11,12]. Furthermore, many dyes and byproducts have been shown to be mutagenic and carcinogenic, as well as xenobiotic and recalcitrant pollutants [12–14]. Therefore, even in small amounts dyes have been reported to pose a serious threat to human health and the environment including the aquatic ecosystem [11]. Other challenges of dye pollution include increasing the chemical oxygen demand (COD) and biological oxygen demand (BOD), compromising the photosynthesis and the aesthetic quality of the water bodies [15,16].

Because dyes are highly soluble in water, some conventional wastewater treatment processes do not effectively remove contaminants [17,18]. Precipitation, coagulation, ion exchange, reverse osmosis, flocculation, membrane filtration, photo electrochemistry, incineration, and other biological, chemical, and physical processes have traditionally been used to treat dye effluents [19]. Nevertheless, because of the excessive

usage of chemicals in some cases, the implementation of these processes may significantly generate secondary metabolites or sludge [20,21]. Furthermore, these traditional methods have been shown to have some drawbacks: high production and maintenance costs, inefficient dye removal, and the potential generation of toxic byproducts [22].

Tartrazine is a dye that is widely used in the food, ink, and pigment industries. Tartrazine has been discovered as a water pollutant in these industries [23,24]. People who are sensitive to tartrazine, a yellow color commonly used in food and medicine, have been linked to allergic reactions to the drug. Individuals with allergic rhinitis, bronchial asthma, urticaria, or sensitivity to nonsteroidal anti-inflammatory drugs have been shown in studies to have significantly lower peak expiratory flow and symptoms such as angioedema, nasal congestion, rhinorrhea, wheezing, itchy skin, and urticaria when given acceptable daily intake doses of tartrazine for seven days [25–30]. In addition, Corder and Buckley's [31] clinical respiratory investigations revealed that tartrazine-sensitive patients experienced bronchoconstriction, resulting in a decrease in respiratory volume. The patients' decreased lung capacity demonstrated this effect. Tartrazine sensitivity is expected to affect approximately 3% of the population, particularly those who are sensitive to salicylates. Tartrazine may cause allergic cross-reactions in some people because its chemical structure is similar to that of benzoates, salicylates, and indomethacin. Tartrazine has also been shown to cause the release of histamine in basophils from people with chronic allergy-related diseases such as urticaria, according to Matsuo and colleagues' research [27]. Furthermore, Baterman and colleagues conducted an experiment with preschool-aged children in which they administered a placebo and then observed their behavior. The findings of this study revealed that artificial dyes, including tartrazine, have a significant impact on the hyperactive behavior of three-year-old children. More recent research has also backed up these findings [32]. The hazardous nature of tartrazine pollution necessitates its removal from the environment. Adsorption is one of the most efficient methods of dye removal from aquatic bodies at dilute levels, with biosorption being a less expensive alternative to expensive sorbents. Bottom Ash is a byproduct of thermal power plants, which burn coke to produce heat and electricity. This material's disposal on the land causes soil infertility [19]. To remove metals [20] and dyes [21,22], It has been investigated as a potential adsorbent. A linearization of the kinetics models has been used in several publications on the sorption of toxicants on bottom ash. Linearization of otherwise nonlinear data can cause the error structure to be disrupted and specific amplified errors to occur at specific regions during linearization because certain linearization causes errors or outliers to be amplified [33]. To that end, we carried out fitting of the sorption of tartrazine to Bottom ash using numerous kinetics model via nonlinear regression.

MATERIALS AND METHODS

Data Acquisition

The digitization software Webplotdigitizer, version 2.5 [34] digitized data from **Figure 3** from a published work [35]. TThis software provides good data extraction accuracy, and its use has been reported in numerous publications [6, 7, 8, and 9]. The data was then nonlinearly regressed using multiple models in the curve-fitting software CurveExpert Professional, Version 2.6.5.

Kinetics models

It is necessary to consider both the kinetic and equilibrium areas when determining the adsorption kinetics constant. Because an incorrect choice of the initial interval time, during which the adsorption occurs very quickly, can result in an incorrect calculation of the rate constant of the PFO and PSO, the adsorption kinetics must be redone using shorter period-times, such as one minute, three minutes, five minutes, and so on. Second, it is common to begin with an insufficient amount of adsorbate or to use a diluted form of it. Not all of the material's adsorption sites are currently being used due to its relatively low initial adsorbate concentration. Because of this distinction, the value of q_e differs from that of q_t. As a result, the values calculated for the parameters of the adsorption kinetic models, particularly the significant rate constants, cannot be accepted [36]. The kinetics model that was evaluated for this investigation may be found in the following (**Table 1**):

Table 1. Kinetic models for fitting the adsorption curve of tartrazine to Bottom ash.

No	Kinetic model	Formula and background	Ref
	Pseudo–first-order	The pseudo-first model was proposed by Lagergren [37,38]. Its valid to about the first 30 min of sorption process [39]. The determination of an adequate q_e value is yet another significant challenge. Notably, the value of q_e after adjustments cannot be lower than the highest value that was observed for q_t [37,38]. The q_e value that was determined via the use of the PFO equation is not the same as the q_e value that was determined through experimentation [40]. It provides more evidence that the PFO equation is unable to adequately model the kinetic adsorption data. It was hypothesized that this disparity was due to the existence of a boundary layer or an external resistance that controlled the initiation of the sorption process [39]. The linearized form has several versions that are incorrect as suggested by Tran [41]. The pseudo–first-order kinetic model equation is as follows [42]: $q_t = q_e(1 - e^{-k_1 t})$ It is the first model that describes the kinetic rate of the liquid-solid phase for the adsorption process based on the adsorption capacity, and it has the distinction of being the first model to do so. It is the kinetic model that has been used the second most frequently to illustrate that the driving force is proportional to the available percentage of active sites. This model provides further evidence that the chemisorption process is at play.	[37,38]
	Pseudo–second-order	The pseudo-second-order model is one that is based on the adsorption capacity onto a solid phase, and Blanchard et al. were the ones who first presented the nonlinear form of the PSO model [43]. It is expressed as: $q_t = \frac{k_2 q e^2 t}{1 + k_2 q_e t}$ Where k_2 (g/(mg.min)) is the pseudo-second-order rate constant The rate of change in adsorption capacity slows down in a manner that is exponentially relative to the quantity of adsorbate that has been adsorbed.	[44]
	Elovich	Simulation of the adsorption of carbon monoxide on the sorbent manganese dioxide was the original driving force behind the development of the Elovich equation. The Elovich model is expressed as follow. $q_t = \frac{1}{\beta ln \alpha \beta} + \frac{1}{\beta ln t}$ Where, α is the initial sorption rate (mg/g.min^{-1}) and β is surface coverage extent (g.mg^{-1}) and chemisorption activation energy. Datapoint that	[45]

starts from the origin (0,0) must be removed due to the *ln* term.

Mixed 1,2-order — A type of pseudo-first-order and pseudo-second-order kinetic equations that is mixed together. This model, which is a linear combination of the pseudo-first-order and the pseudo-second-order equations, is referred to as the mixed 1,2-order equation (MOE). The formula is as follow. [46,47]

$$q_t = q_e\left\{1 - \frac{k_1 exp(-k_1 t)}{k_1 + q_e k_2\left(1 - exp(-k_1 t)\right)}\right\}$$

Where k_1 and k_2, represent first- and second-order kinetics, respectively.

Fractal-like pseudo-first order — Incorporating the fractal concept into the pseudo-first-order model was one of the suggested modifications to the model. The formula is as follow. [48]

$$q_t = q_e\left[1 - exp\left(-k_1' t^{\phi}\right)\right]$$

Here the adsorption rate coefficient might have a temporal dependency during the adsorption time. ϕ is the fractal time exponent and k'_1 (1/min$^{\phi}$) is the fractal-like pseudo-first-order rate constant.

Fractal-like pseudo-second order — In a similar vein, an additional modification for the pseudo-second-order model has been suggested, and this time it involves the concept of fractals. The formula is as follow. [48]

$$q_t = \frac{k_2' {q_e}^2 t^{\phi}}{1 + k_2' q_e t^{\phi}}$$

k'_2 (g/(mg min))$^{\phi}$ and ϕ are the fractal-like pseudo-second-order rate constant and exponent, respectively.

Pseudo-nth order — It can be difficult to discern the order of the adsorption process in particular circumstances. This indicates that the PSO and PFO models are able to adequately fit the experience data of time dependency. Because of this, the pseudo-nth-order (PNO) model or the general order kinetic (GOK) model is also utilized in order to accurately identify the overall order of the adsorption process. [49]

$$q_t = q_e - \frac{q_e}{[k_N (q_e)^{n-1} t(n-1) + 1]^{\frac{1}{1-n}}}; n \neq 1$$

Where,
n is the order of kinetic adsorption (n could be an integer or non-integer rational number) and k_N is the general order rate constant ((g/mg)$^{n-1}$/min),

One-site Langmuir — The kinetic model works on the assumption that the overall adsorption rate is simply the difference between the adsorption and desorption rates, and that once equilibrium is reached, these two rates cancel each other out to give the same result. While the rate of desorption is related to the amount that was adsorbed, the rate of adsorption is proportional to the solute concentration that is already present in the bulk phase and the amount of accessible adsorbent surface. The formula is as follow. [50]

$$q_t = q_e\left[\frac{K'_{ad}}{(K'_{ad} + K_d)}\right]\{1 - exp[-(K'_{ad} + K_d)t]\}$$

k'_{ad} is the Langmuir adsorption rate constant (1/min) and k_d is the desorption rate constant (1/min)

Modified-Freundlich — The Freundlich equation was modified to include a time-dependent expression, which allowed for the development of a kinetic model. The formula is as follow. [51]

$$q_t = kC_0 t^{\frac{1}{n}}$$

where k is the apparent adsorption rate constant (L/g.min$^{1/n}$); n is the Kuo-Lotse constant; C_0 is the initial adsorbate concentration (mmol/L); and t is the adsorption time

Avrami — Under the premise that nucleation occurs in a manner that is spatially random, this model predicts the kinetics of phase transition. This provides an illustration of the kinetic parameters as feasible variations of the adsorption rates in terms of the initial concentration and the adsorption period. Additionally, it provides an evaluation of fractional kinetic orders. The formula is as follow. [52]

$$q_t = q_e\{1 - exp[-(k_{Av} t)]^{n_{Av}}\}_v$$

the Avrami kinetic model rate constant (1/min) and n_{Av} (fraction) is the model exponent of time related to the adsorption mechanism changes.

Exponential — An exponential form of the kinetic equation is a form of the equation that can be used to illustrate the pattern of an adsorption rate as a function of time. Between pseudo-first-order models and pseudo-second-order models is where the driving force of the exponential model rests. Both homogeneous and heterogeneous surfaces are appropriate contexts for using the kinetic model. The formula is as follow. [53]

$$\frac{q_t}{q_e} = ln\left[2.72 - 1.72 exp\left(-k_{Exp} t\right)\right]$$

k_{Exp} is the exponential kinetic model rate constant (mg/(g.min)). Datapoint that starts from the origin (0,0) must be removed due to the *ln* term.

Double-exponential — Wilczak and Keinath came up with a double exponential kinetic model after observing the kinetics of copper(II) and lead(II) adsorption on activated carbon. This model was based on their results. This equation describes the adsorption characteristics as a two-step mechanism, with the first step being a quick phase that includes both internal and exterior diffusions. This is preceded by a slow phase that is governed by the intra-particle diffusion. The formula is as follow. [54]

$$q_t = q_e - \frac{D_R}{m_{ads}} exp(-k_{DR} t) - \frac{D_S}{m_{ads}} exp(-k_{DS} t)\}$$

Where,
K_{DR} and K_{DS} are diffusion parameters (1/min) for the rapid and slow step of double-exponential model, respectively, m_{ads} is the adsorbent amount in the solution (g/L) and D_R and D_S are adsorption rate parameters of the rapid and the slow step (mmol/L), respectively.

Hyperbolic tangent — The hyperbolic tangent function has been used as the foundation for the development of this mathematical model. In addition to this, it is able to calculate the precise equilibrium time of the adsorption process. The formula is as follow. [55]

$$\frac{q_t}{q_e} = \left[tanh\left(\pi \frac{t}{t_{eHT}}\right)\right]^{n_{HT}}$$

t_{eHT} is the required time for adsorption to reach the equilibrium state (min) and n_{HT} represents the adsorbent surface heterogeneity.

Brouers and Sotolongo — a time dependent rate or hazard function (in reliability theory) or intensity of transition (in relaxation theory), $R(t)$. The formula is as follow. [57]

$$y = qe\left[1 - \left(1 + (n-1)\left(\frac{t}{\tau}\right)^{\alpha}\right)^{-\frac{1}{n-1}}\right]$$

Musawi suggests to use (n, a) of (1.5, a). The formula is as follow.

$$y = q_e\left[1 - \left(1 + (0.5)\left(\frac{t}{\tau}\right)^{\alpha}\right)^{-2}\right]$$

	Where n is the reaction's fractional order; α is the fractal coefficient that, on a macro scale, expresses the level of complexity of the sorbent-sorbate relationship, and τ is the characteristic time (min). It has been suggested for the whole series to use B_{Sf} (1.5,a) [56].	
normalized Gudermannian function	In order to simulate the sigmoidal shape of sorption kinetics data, the normalized Gudermannian function was introduced. The function is related to both the circular and the hyperbolic functions. The formula is as follow. $\frac{q_t}{q_e} = \left\{0.637 tan^{-1}\left[sinh \frac{5.233 \times t}{t_{eG}}\right]\right\}^{n_G}$ where where t_{eG} reflects the amount of time that must have passed for the adsorption process to reach the condition of equilibrium and the heterogeneity of the adsorption system is represented by the parameter n_G.	[58]
Sigmoidal Chapman	In addition to that, the Sigmoidal Chapman model was incorporated into this study. It is depicted by the equation: where the adsorption rate constant is denoted by b (h^{-1}), and c represents how the adsorption rate varies as a function of time. The formula is as follow. $q_t = q_e(1 - e^{-bt})^c$ The idea that adsorbate molecules interact with one another in a cooperative manner forms the foundation of the equivalent Chapman isotherm model.	[59]

Note
q_e is the time dependent and maximum sorbed quantities (mg/g)
t is time (min)

Statistical analysis

To determine if there is a significant difference in terms of fitness among models with varying numbers of parameters, statistics functions such as the adjusted coefficient of determination *(adjR^2)*, Root-Mean-Square Error (RMSE), corrected Akaike Information Criterion (AICc), Bayesian Information Criterion (BIC), Hannan-Quinn Information Criterion (HQC), bias factor, and accuracy factor (BF, AF) were applied to the same set of experimental data. The RMSE, which accounts for the penalty for the number of parameters, was calculated using Eqn 1, where n is the number of experimental data, p is the number of parameters, Ob_i is the experimental data, and Pd_i is the value predicted by the model [60].

$$RMSE = \sqrt{\frac{\sum_{i=1}^{n}(Pd_i - Ob_i)^2}{n-p}} \qquad \text{(Eqn. 1)}$$

To determine the validity of the models, both BF and AF were used. The Bias Factor should be set to 1 to achieve a correlation of 1 between the predicted and observed values. If the Bias Factor (as shown in Equation 2) is greater than 1, it indicates a fail-safe model, and if it is less than 1, it indicates a fail-negative model. If Accuracy is less than 1, it means that the prediction will be less accurate (Eqn. 3).

$$Bias\ factor = 10\left(\sum_{i=1}^{n} log\frac{(Pd_i/Ob_i)}{n}\right) \qquad \text{(Eqn. 2)}$$

$$Accuracy\ factor = 10\left(\sum_{i=1}^{n} log\frac{|(Pd_i/Ob_i)|}{n}\right) \qquad \text{(Eqn. 3)}$$

In linear regression, the best fitting model was determined by R^2 or coefficient of determination. However, in nonlinear regression, the R^2 does not give a comparative analysis where the number of parameters between models is different.

To overcome this, adjusted R^2 was used to calculate the quality of the nonlinear models. In the adjusted R^2 formula, S_y^2 is the total variance of the y-variable and RMS is Residual Mean Square (Eqns. 4 and 5).

$$Adjusted\ (R^2) = 1 - \frac{RMS}{S_Y^2} \qquad \text{(Eqn. 4)}$$

$$Adjusted\ (R^2) = 1 - \frac{(1-R^2)(n-1)}{(n-p-1)} \qquad \text{(Eqn. 5)}$$

Various statistical models can be evaluated for a given range of experimental data using the Akaike Information Criterion (AIC). Alternatively, AICc (the corrected AIC) should be used for data sets with numerous parameters or a few data point values [61]. The AICc was calculated based on the following Eqn. 6.

$$AICc = 2p + n1n\left(\frac{RSS}{n}\right) + 2(p+1) + \frac{2(p+1)(p+2)}{n-p-2} \qquad \text{(Eqn. 6)}$$

The AICc gives information about the differences that exist between the two models in terms of the number of parameters (p) and the fitting. The AICc value that is the smallest possible would suggest the model that best fits the data [61]. A further information-theory-based approach to statistics is the Bayesian Information Criterion (Eqn. 7). The number of parameters is punished more harshly by this error function than it is by AIC [62].

$$BIC = n.\ln\frac{RSS}{n} + p.\ln(n) \qquad \text{(Eqn. 7)}$$

The Hannan–Quinn information criterion, often known as the HQC, is an additional error function approach that relies on the information theory (Eqn. 8). In contrast to the AIC, the HQC exhibits a high level of consistency because the equation contains the *ln ln* n term. [63];

$$HQC = n \times ln\frac{RSS}{n} + 2 \times p \times ln(\ln n) \qquad \text{(Eqn. 8)}$$

Another is MPSD. The Marquardt's percent standard deviation (MPSD). This error function distribution follows the geometric mean error which allows for the penalty to the number of parameters of a model (Eqn. 9).

$$MPSD = 100\sqrt{\frac{1}{n-p}\sum_{i=1}^{n}\left(\frac{Ob_i - Pd_i}{Ob_i}\right)^2} \qquad \text{(Eqn. 9)}$$

where n is the number of experimental data, p is the number of parameters, Ob_i is the experimental data, and Pd_i is the value predicted by the model

RESULTS AND DISCUSSION

Determination of kinetic model for batch adsorption studies

Since the linearisation of nonlinear data disturbs the data's error structure, this makes it harder to assess uncertainty, which is often reported as 95% confidence interval range [64]. Hence, the non–linear regression is preferable for kinetic model fitting since it is conducted on the same abscissa with a linear regression plot, showing more accurate calculations. The various kinetic models utilized in this study (**Figs. 1** to **16**) shows visually acceptable fittings with the exception of the one-site Langmuir model (**Fig. 8**) for all tested models.

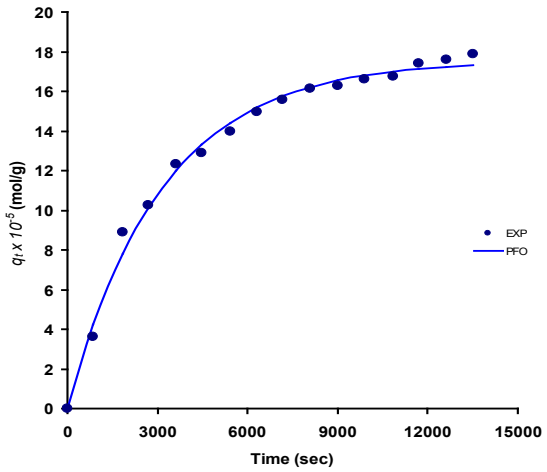

Fig. 1. Experimental data versus calculated data (line) of tartrazine dye adsorption using Bottom ash as modelled using the pseudo-first order model.

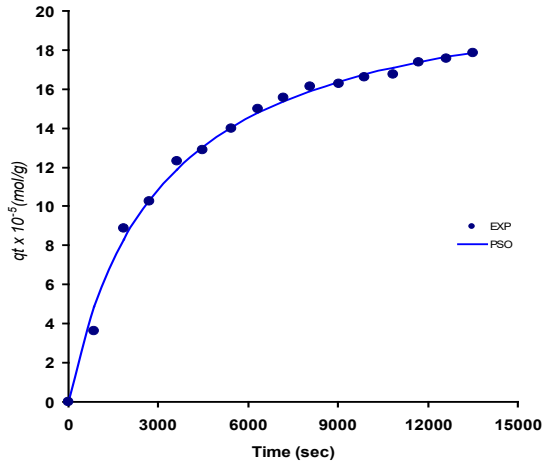

Fig. 2. Experimental data versus calculated data (line) of tartrazine dye adsorption using Bottom ash as modelled using the pseudo-second order model.

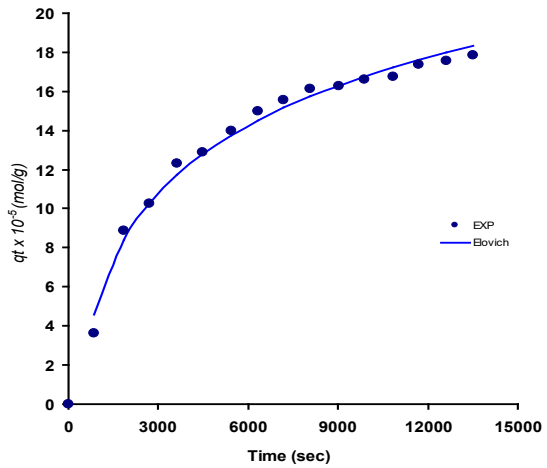

Fig. 3. Experimental data versus calculated data (line) of tartrazine dye adsorption using Bottom ash as modelled using the Elovich model.

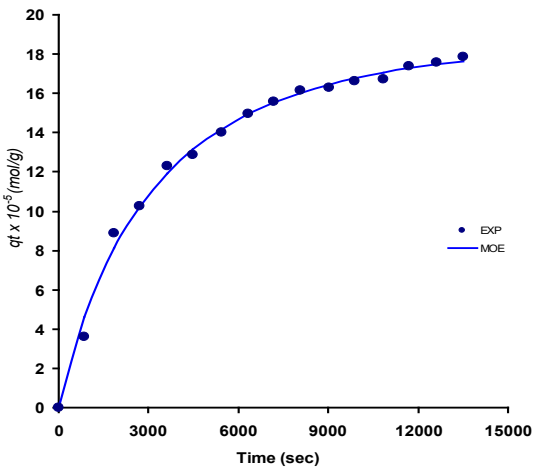

Fig. 4. Experimental data versus calculated data (line) of tartrazine dye adsorption using Bottom ash as modelled using the mixed order (MOE) model.

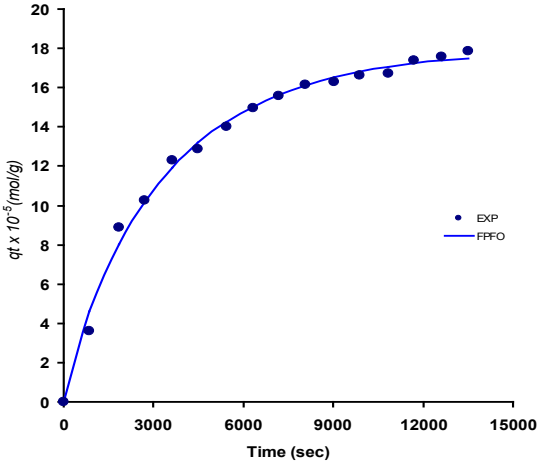

Fig. 5. Experimental data versus calculated data (line) of tartrazine dye adsorption using Bottom ash as modelled using the fractal pseudo-first order model.

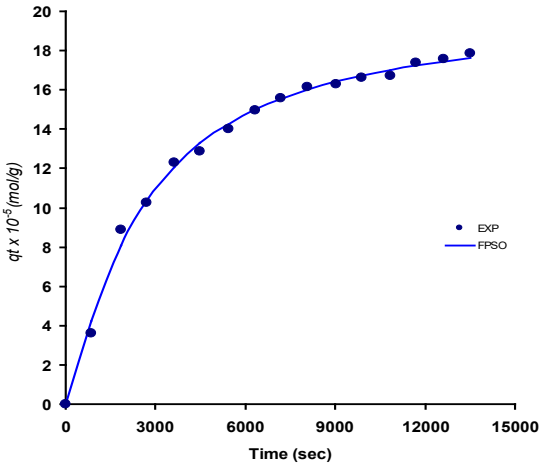

Fig. 6. Experimental data versus calculated data (line) of tartrazine dye adsorption using Bottom ash as modelled using the fractal pseudo-second order model.

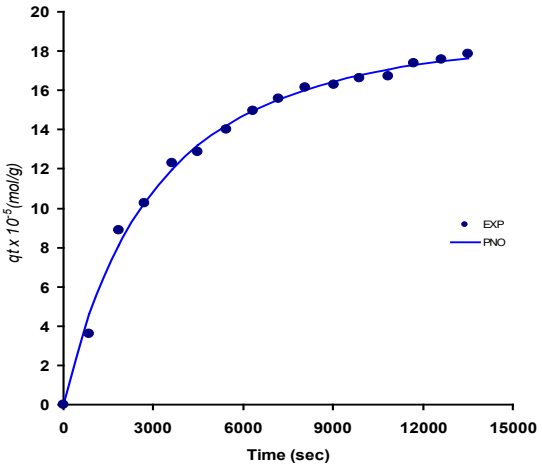

Fig. 7. Experimental data versus calculated data (line) of tartrazine dye adsorption using Bottom ash as modelled using the fractal pseudo-nth order model.

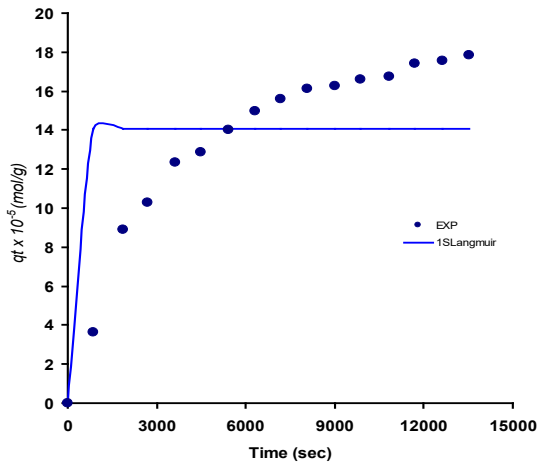

Fig. 8. Experimental data versus calculated data (line) of tartrazine dye adsorption using Bottom ash as modelled using the one-site Langmuir model.

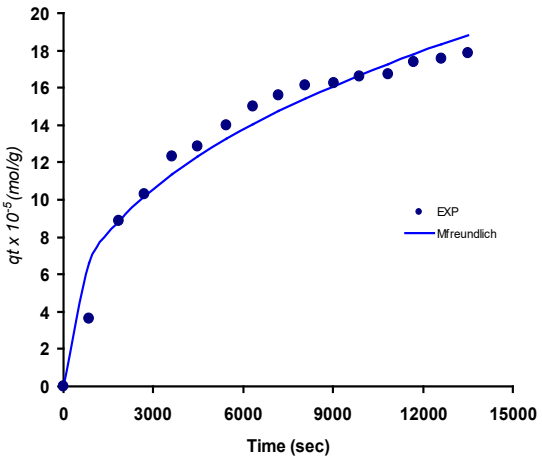

Fig. 9. Experimental data versus calculated data (line) of tartrazine dye adsorption using Bottom ash as modelled using the modified Freundlich model.

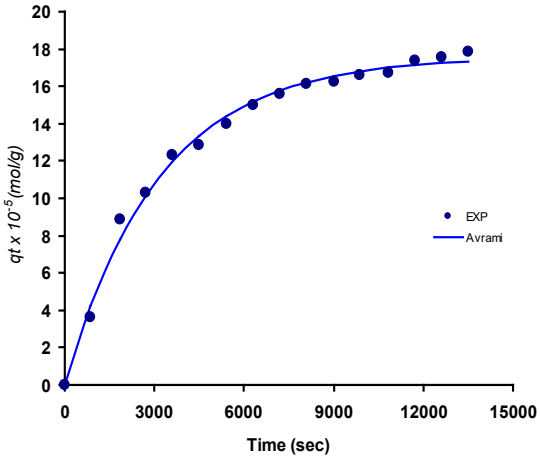

Fig. 10. Experimental data versus calculated data (line) of tartrazine dye adsorption using Bottom ash as modelled using the Avrami model.

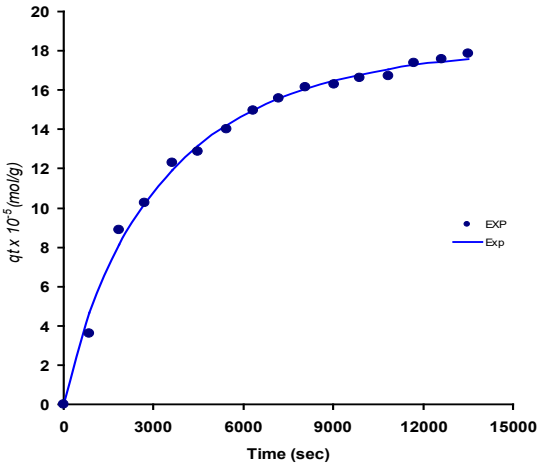

Fig. 11. Experimental data versus calculated data (line) of tartrazine dye adsorption using Bottom ash as modelled using the exponential model.

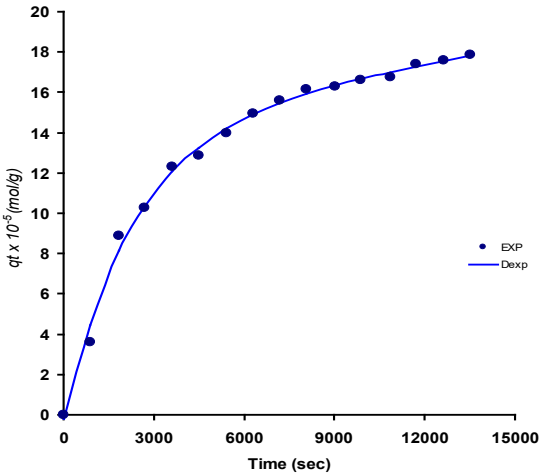

Fig. 12. Experimental data versus calculated data (line) of tartrazine dye adsorption using Bottom ash as modelled using the double-exponential model.

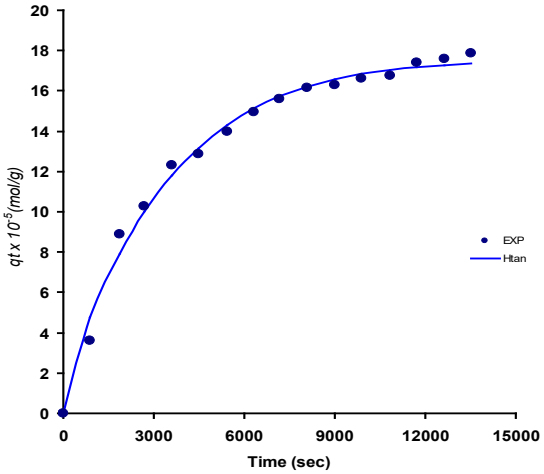

Fig. 13. Experimental data versus calculated data (line) of tartrazine dye adsorption using Bottom ash as modelled using the hyperbolic tangent model.

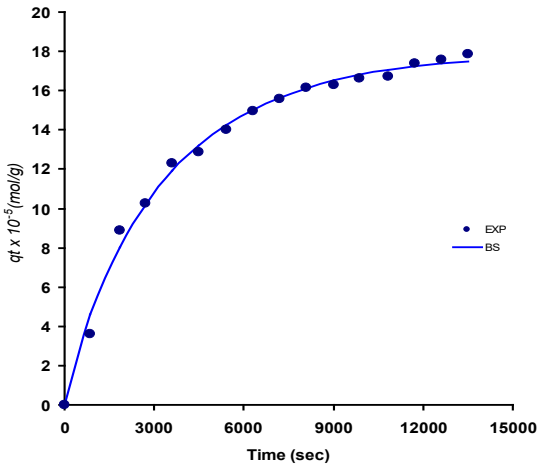

Fig. 14. Experimental data versus calculated data (line) of tartrazine dye adsorption using Bottom ash as modelled using the Brouers and Sotolongo model.

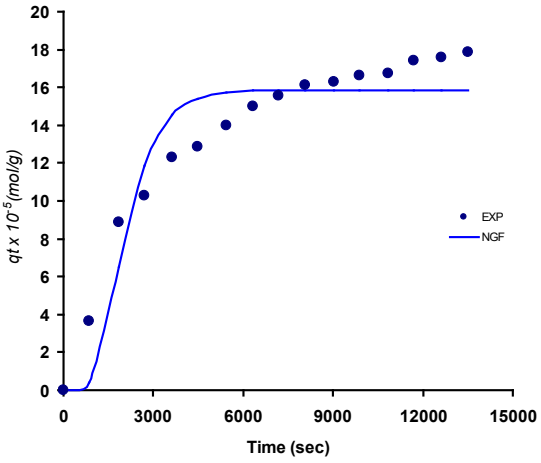

Fig. 15. Experimental data versus calculated data (line) of tartrazine dye adsorption using Bottom ash as modelled using the normalized Gudermannian function model.

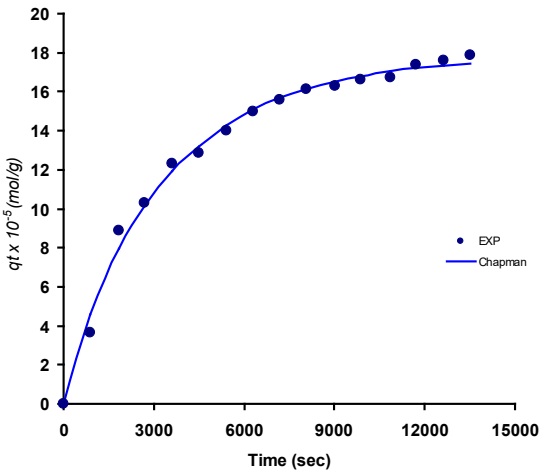

Fig. 16. Experimental data versus calculated data (line) of tartrazine dye adsorption using Bottom ash as modelled using the sigmoidal Chapman model.

The pseudo-second order was the best model based on the Bias and Accuracy factor near unity, but based on other error function analysis, this model performs equally well with the exponential and fractal-like pseudo-second order based other error functions such as *RMSE, adjR*^{2}*, MPSD, BIC, HQC,* and especially the AICc function as the absolute difference is 5 absolute unit making discriminatory activity difficult. Furthermore, because the pseudo-second order and exponential models have only two parameters, they are less complicated according to Occam's razor (**Table 2**).

Due to the popularity and numerous applications of the pseudo-second order model compared to the less well-known exponential model; we chose the pseudo-2nd order model as the bets model fitting the sorption of tartrazine to Bottom ash. Kinetic analysis using the PSO model gave a value of equilibrium adsorption capacity, q_e of 21.88 mg g^{-1} (95% confidence interval (C.I.), 20.93 to 22.84) and k_2 (g/(mg.sec)) of 0.00002 (95%, C.I., 0.00001 to 0.00002) (**Table 2**).

The result of the nonlinear regression work was within the range of the original study at 9.28 mg g^{-1} and 0.026 As far as tartrazine biosorption is concerned (**Table 4**), the PSO model is also the best model for several adsorbents such as *Inula viscosa* waste [65], activated carbon derived from *Cassava sievate* biomass [66], iron nanoadsorbents utilizing different waste plant biomass [67], lanthanum enriched aminosilane-grafted mesoporous carbon material [68], magnetic Ni-Ag bimetallic nanoparticles supported on reduced graphene oxide (Ni-Ag NPs/rGO) [69], activated carbon produced from pecan nut shells [70], masau stone (MS) [71], copper coordinated dithiooxamide metal-organic framework (Cu-DTO MOF) [72], Fe(II) based adsorbent system [73], iron modified zeolitic tuff [74], activated carbon from Alligator weed (*Alternenthera philoxeroids*) [75], polyaniline nanolayer composite [76], while the PFO was the best model for adsorption of tartrazine using natural quartz, modified with a cationic surfactant and homoionized with sodium [77] ZnAl-LDH/PVA nanocomposite [78]. The ability to fit kinetic data was widely accepted as the best test of the validity of the PFO and PSO equations, despite the fact that such a test has little to do with whether or not the equations have a solid physicochemical foundation.

Table 2. Statistical analysis for tartrazine adsorption using Bottom ash adsorbent at 100 mg/L dye.

Model	p	RMSE	adR^2	MPSD	AICc	BIC	HQC	BF	AF
One-site Langmuir	3	4.10	-0.469	29.11	59.45	50.13	47.94	0.91	1.11
Normalized Gudermannian	3	1.85	0.879	224.9	33.97	24.65	22.45	0.98	1.04
Modified-Freundlich	2	1.02	0.955	12.81	10.39	3.93	2.47	1.00	1.01
Double exponential	5	0.39	0.994	6.34	-4.53	-22.01	-25.67	1.00	1.00
Hyperbolic tangent	3	0.51	0.989	7.73	-7.10	-16.42	-18.62	1.00	1.01
Avrami	3	0.46	0.991	5.84	-10.51	-19.83	-22.02	1.00	1.01
Sigmoidal Chapman	3	0.44	0.992	6.70	-11.84	-21.16	-23.35	1.00	1.01
Brouers and Sotolongo	3	0.43	0.992	6.74	-12.69	-22.01	-24.21	1.00	1.01
Fractal-like PFO	3	0.43	0.992	6.74	-12.69	-22.01	-24.21	1.00	1.01
Mixed 1,2-order	3	0.40	0.993	6.68	-14.93	-24.25	-26.45	1.00	1.01
Pseudo-nth order	3	0.39	0.994	6.50	-15.71	-25.03	-27.23	1.00	1.01
Elovich	2	0.45	0.992	6.29	-15.84	-22.30	-23.76	1.00	1.01
Pseudo-first order (PFO)	2	0.44	0.992	103.5	-16.14	-22.60	-24.06	1.00	1.01
Pseudo-second order (PSO)	2	0.41	0.993	7.17	-18.55	-25.01	-26.47	1.00	1.00
Fractal-like PSO	3	0.34	0.995	4.99	-19.91	-29.23	-31.43	1.00	1.01
Exponential	2	0.39	0.994	6.50	-19.95	-26.41	-27.87	1.00	1.01

Table 3. Model constants for the top-three kinetic models for tartrazine adsorption using Bottom ash adsorbent at 100 mg/L dye.

Model	value	(95% C.I.)
Pseudo-2nd order		
q_e (mg/g)	21.88	20.93 to 22.84
k_2 (g/(mg.sec))	0.00002	0.00001 to 0.00002
Exponential		
q_e (mg/g)	18.25	17.68 to 18.82
k_{Exp} (mg/(g.sec))	0.00021	0.00019 to 0.00023
Fractal-like Pseudo-2nd Order		
q_e (mg/g)	19.85	18.52 to 21.19
k'_2 (g/(mg sec))$^{\phi}$	0.000003	-0.000001 to 0.000008
ϕ	1.25	1.037 to 1.414

Both k_1 and k_2 were phenomenological rate constants that decreased when the initial adsorbate concentration was increased. The values of k_1 and k_2 varied greatly between measurements, making it difficult to draw conclusions about the underlying physics and chemistry and extrapolate valuable results. Even if the experimental conditions affecting the adsorption kinetics were not completely controlled, the PFO and PSO equations can be fitted to most kinetic data. The PFO equation consistently produced lower estimates of q_e than the experiments. This mismatch was caused by a delay in the adsorption process, which was most likely caused by the presence of a boundary layer or external resistance regulating. The chemical reaction is not always the rate-limiting step in the adsorption process that followed the PSO equation because a good fit alone does not reveal the true nature of the rate-limiting step [47,79,80].

To determine whether the adsorption of pollutants in solution is a physical or chemical process, analytical methods as well as data on adsorptive thermodynamics such as changes in entropy and enthalpy, activation- and adsorption energies are required [41]**.** Both kinetic models for sorption from liquid solutions were obtained without considering any process conditions to be particularly important. Azizian presents the creation of these models from theory in detail, with experimental findings supporting his analysis. The theoretical derivation of the model has the advantage of providing an estimate of the circumstances required to provide a more expressive interpretation of kinetic parameters. This is possible because the models can predict the conditions that must be met. Azizian has noticed that the PFO kinetic model's observed rate constant (k_1) symbolizes a mix of desorption and adsorption rate constants, and not the rate constant's intrinsic adsorption [81].

This is because k_1 does not the rate constant's intrinsic adsorption. The PFO model can account for the use of high starting solute concentration (C_0) of the adsorbate in the study of sorption kinetics, but the PSO model can more consistently suit low values of C_0. The PFO model can account for the use of low C_0 values as well. The observed k_1 value is linearly proportionate to the initial solute concentration for adsorption profiles that obey the PFO kinetic model, where the intercept and slope imply the desorption and adsorption rate constants, respectively. This holds true for adsorption profiles that adhere to the PFO kinetic model. In the scenario where adsorption processes follow PSO kinetics, the observed rate constant is a convoluted function of the initial sorbate concentration [81].

To reiterate, when the solute's initial concentration is high, experimental studies support the PFO model. When the solute concentration is low, the PSO kinetic model takes precedence [81–86]. Furthermore, the intraparticle diffusion model is one of several kinetic adsorption models that have been used to investigate the adsorption process at the atomic and molecular levels, particularly for porous sorbents [87,88]. When chemical sorption or chemisorption is assumed to be the rate-limiting phase, the PSO kinetic model can predict behavior over the entire adsorption range. As a result, the adsorption rate is independent of the adsorbate concentration and is instead determined by the adsorption capacity. This model can calculate equilibrium adsorption capacity, which is a significant improvement over the Lagergren first order model. As a result, there is no need to use experimental data to determine the adsorption equilibrium capacity. As the initial solute concentration increases, the correlation between the data and the PSO kinetics model decreases, while the data and the PFO model become increasingly well-fitted [81].

Table 4. Summary of tartrazine dye sorption by sorbents.

Adsorbent	Best kinetics	Ref
Inula viscosa waste	PSO	[65]
activated carbon derived from *Cassava sievate* biomass	PSO	[66]
iron nanoadsorbents utilizing different waste plant biomass	PSO	[67]
lanthanum enriched aminosilane-grafted mesoporous carbon material	PSO	[68]
magnetic Ni-Ag bimetallic nanoparticles supported on reduced graphene oxide (Ni-Ag NPs/rGO)	PSO	[69]
activated carbon produced from pecan nut shells	PSO	[70]
Copper coordinated dithiooxamide metal-organic framework (Cu-DTO MOF)	PSO	[72]
Fe(II) based adsorbent system	PSO	[73]
iron modified zeolitic tuff	PSO	[74]
activated carbon from Alligator weed (*Alternenthera philoxeroids*)	PSO	[75]
polyaniline nanolayer composite	PSO	[76]
masau stone (MS)	PSO	[71]
Activated carbon of *Lantana camara*	PSO	[89]
Crosslinked Chitosan-Coated Bentonite	PSO	[90]
natural quartz, modified with a cationic surfactant and homoionized with sodium	PFO	[77]
ZnAl-LDH/PVA nanocomposite	PFO	[78]
hen feathers	PFO	[35]
Deoiled soya waste	PFO (default)	[91]
Bottom ash from thermal power	PFO (default)	[91]
Chitin and Chitosan	Avrami	[92]

Note:
PSO Pseudo-2nd order
PFO Pseudo-1st order

CONCLUSION

Linearized adsorption kinetics has drawbacks such as inaccurate representation of the parameters' 95% confidence interval output, unbalanced attention to potential outliers, and magnification of errors may result in inaccurate parameter values. In this study, we used nonlinear regression to investigate 16 adsorption kinetics models of tartrazine by bottom ash. The pseudo-second order was the best model based on the Bias and Accuracy factor near unity, but based on other error function analysis, this model performs equally well with the exponential and fractal-like pseudo-second order based other error functions such as *RMSE, adjR*^{2}*, MPSD, BIC, HQC*, and especially the *AICc* function as the absolute difference is 5 absolute unit making discriminatory activity difficult. Furthermore, because the pseudo-second order and exponential models have only two parameters, they are less complicated according to Occam's razor. Because the pseudo-second order model is more popular and has more applications than the less well-known exponential model, we chose it as the best model for tartrazine sorption to Bottom ash. Kinetic analysis using the PSO model gave a value of equilibrium adsorption capacity, q_e of 21.88 mg g^{-1} (95% confidence interval (C.I.), 20.93 to 22.84) and k_2 (g/(mg.sec)) of 0.00002 (95%, C.I., 0.00001 to 0.00002).

REFERENCES

1. Jayanth N, Karthik R, Logesh S, K SR, Vijayanand K. Environmental issues and its impacts associated with the textile processing units in. 2nd Int Conf Environ Sci Dev IPCBEE. 2011;4(17):120–4.
2. Kurade MB, Awasthi MK, Govindwar SP, Jeon BH, Kalyani D. Editorial: Microbiotechnology Tools for Wastewater Cleanup and Organic Solids Reduction. Front Microbiol. 2021;12(February):10–2.
3. Singh KP, Gupta S, Singh AK, Sinha S. Optimizing adsorption of crystal violet dye from water by magnetic nanocomposite using response surface modeling approach. J Hazard Mater. 2011;186(2–3):1462–73.
4. Chavan RB. Indian textile industry - Environmental issues. Indian J Fibre Text Res. 2001;26(1–2):11–21.
5. Kalme SD, Parshetti GK, Jadhav SU, Govindwar SP. Biodegradation of benzidine based dye Direct Blue-6 by Pseudomonas desmolyticum NCIM 2112. Bioresour Technol. 2007;98(7):1405–10.
6. Kumar P, Bhati H, Rani A, Singh R. Role of Biosorption of Dyes and Microorganisms in Environment. Life Sci. 2015;4(2):38–41.
7. Mohan S, Muralimohan N, Vidhya K, Sivakumar CT. a Case Study on-Textile Industrial Process, Characterization and Impacts of Textile Effluent. Indian JSciRes. 2017;17(1):80–084.
8. Islam MM, Mahmud K, Faruk O, Billah S. Assessment of environmetal impacts for textile dyeing industries in Bangladesh. Proc Int Conf Green Technol Environ Conserv GTEC-2011. 2011;2(6):173–81.
9. Izuan M, Halmi E, Gunasekaran B, Razi Othman A, Dahalan FA. A rapid inhibitive enzyme assay for monitoring heavy metals pollution in the Juru Industrial Estate [Internet]. Vol. 3, Bioremediation Science and Technology Research. 2015 [cited 2021 Jun 11]. p. 7–12. Available from: http://journal.hibiscuspublisher.com/index.php/BSTR/index
10. Manogaran M, Yasid NA, Othman AR, Gunasekaran B, Izuan M, Halmi E, et al. Biodecolourisation of Reactive Red 120 as a Sole Carbon Source by a Bacterial Consortium-Toxicity Assessment and Statistical Optimisation. Public Health. 2021;18:2424.
11. Lellis B, Fávaro-polonio CZ, Pamphile JA, Polonio JC. Effects of textile dyes on health and the environment and bioremediation potential of living organisms. 2019;
12. Puvaneswari N, Muthukrishnan J, Gunasekaran P. Toxicity assessment and microbial degradation of azo dyes. Indian J Exp Biol. 2006;44(8):618–26.
13. Karim ME, Dhar K, Hossain MT. Decolorization of Textile Reactive Dyes by Bacterial Monoculture and Consortium Screened from Textile Dyeing Effluent. J Genet Eng Biotechnol. 2018;16(2):375–80.
14. Şenol ZM. Effective biosorption of Allura red dye from aqueous solutions by the dried-lichen (Pseudoevernia furfuracea) biomass. Int J Environ Anal Chem. 2020;00(00):1–15.
15. El-Idreesy TT, Khoshala O, Firouzi A, Elazab HA. Equilibrium and kinetic study on the biosorption of trypan blue from aqueous solutions using avocado seed powder. Biointerface Res Appl Chem. 2021;11(3):11042–53.
16. Walker GM, Weatherley LR. Biodegradation and biosorption of acid anthraquinone dye. Environ Pollut. 2000;219–23.
17. Vijayaraghavan K, Yun Y sang. Utilization of fermentation waste (Corynebacterium glutamicum) for biosorption of Reactive Black 5 from aqueous solution. 2007;141:45–52.
18. Vijayaraghavan K, Yun YS. Bacterial biosorbents and biosorption. Biotechnol Adv. 2008;26(3):266–91.
19. Wang Y, Jiang L, Shang H, Li Q, Zhou W. Environmental Technology & Innovation Treatment of azo dye wastewater by the self-flocculating marine bacterium Aliiglaciecola lipolytica. Environ Technol Innov. 2020;19:100810.
20. Chang JS, Chou C, Lin YC, Lin PJ, Ho JY, Lee Hu T. Kinetic characteristics of bacterial azo-dye decolorization by Pseudomonas luteola. Water Res. 2001;35(12):2841–50.
21. Lade H, Kadam A, Paul D, Govindwar S. A Low-Cost Wheat Bran Medium for Biodegradation of the Benzidine-Based Carcinogenic Dye Trypan Blue Using a Microbial Consortium. 2015;3480–505.
22. Ismail M, Akhtar K, Khan MI, Kamal T, Khan MA, M. Asiri A, et al. Pollution, Toxicity and Carcinogenicity of Organic Dyes and their Catalytic Bio-Remediation. Curr Pharm Des. 2019;25(34):3645–63.
23. Shiralipour R, Larki A. Pre-concentration and determination of tartrazine dye from aqueous solutions using modified cellulose nanosponges. Ecotoxicol Environ Saf. 2017 Jan 1;135:123–9.
24. Methneni N, González JAM, Van Loco J, Anthonissen R, de Maele JV, Verschaeve L, et al. Ecotoxicity profile of heavily contaminated surface water of two rivers in Tunisia. Environ Toxicol Pharmacol. 2021 Feb 1;82:103550.
25. Bateman B, Warner JO, Hutchinson E, Dean T, Rowlandson P, Gant C, et al. The effects of a double blind, placebo controlled, artificial food colourings and benzoate preservative challenge on hyperactivity in a general population sample of preschool children. Arch Dis Child. 2004 Jun 1;89(6):506–11.
26. Doguc D, Aktas A, Gazioglu N, Kocabas CN. Tartrazine and other azo dyes: a review of literature. Food Chem Toxicol. 2013;62:340–50.
27. Matsuo H, Kato K, Ohno Y, Kato S. The effect of tartrazine on histamine release from human basophils. Allergol Int. 2013;62(4):539–47.
28. Khayyat MA, Al-Qahtani JA, Al-Saleh YA, Al-Mofleh IA. The prevalence of food additives intolerance in adult patients with chronic urticaria. Int J Dermatol. 2017;56(5):536–41.
29. Bhatt S, Kamat D. The Role of Tartrazine in the Development of Asthma and Allergic Rhinitis in Children. J Allergy Clin Immunol Pract. 2018;6(4):1251–8.
30. Ara&uacute L, Caldas J, Fl&aacute, Marmo VC, Patr&iacute, Costa CD, et al. Hormesis in tartrazine allergic responses of atopic patients: An overview of clinical trials and a raw data revision. Environ Dis. 2020 Jul 1;5(3):59–59.
31. Corder R, Buckley D. Tartrazine and respiratory symptoms. Thorax. 1995;50(6):663–6.
32. Yong SB, Gau SY, Guo YC, Wei JCC. Allergy from perspective of environmental pollution effects: from an aspect of atopic dermatitis, immune system, and atmospheric hazards—a narrative review of current evidences. Environ Sci Pollut Res. 2022 Aug 1;29(38):57091–101.
33. González-López ME, Laureano-Anzaldo CM, Pérez-Fonseca AA, Arellano M, Robledo-Ortíz JR. A Critical Overview of Adsorption Models Linearization: Methodological and Statistical Inconsistencies. Sep Purif Rev. 2021 Aug 1;0(0):1–15.
34. Rohatgi A. WebPlotDigitizer User Manual. HttparohatgiinfoWebPlotDigitizerapp Accessed June 2 2014. 2013;1–17.
35. Mittal A, Kurup L, Mittal J. Freundlich and Langmuir adsorption isotherms and kinetics for the removal of Tartrazine from aqueous

solutions using hen feathers. J Hazard Mater. 2007;146(1–2):243–8.
36. Tran H. Differences between Chemical Reaction Kinetics and Adsorption Kinetics: Fundamentals and Discussion. 2022 Jun 22;
37. Lagergren, S. About the theory of so-called adsorption of soluble substances. Kongliga Sven Vetenskapsakademiens Handl. 1898;24(4):1–39.
38. Ho YS, Mckay G. Sorption of Dye From Aqueous Solution by Peat. Chem Eng J. 1998 Jun 1;70:115–24.
39. Ho YS, McKay G. The kinetics of sorption of basic dyes from aqueous solution by sphagnum moss peat. Can J Chem Eng. 1998;76(4):822–7.
40. Febrianto J, Kosasih AN, Sunarso J, Ju YH, Indraswati N, Ismadji S. Equilibrium and kinetic studies in adsorption of heavy metals using biosorbent: A summary of recent studies. J Hazard Mater. 2009;162(2–3):616–45.
41. Tran HN, You SJ, Hosseini-Bandegharaei A, Chao HP. Mistakes and inconsistencies regarding adsorption of contaminants from aqueous solutions: A critical review. Water Res. 2017 Sep 1;120:88–116.
42. Lagergren S, Svenska K. , "About the theory of so-called adsorption of soluble substances, Zur theorie der sogenannten adsorption gel?ster stoffe,." Vetenskapsakademiens Handl. 1898;24:1–39.
43. Blanchard G, Maunaye M, Martin G. Water Res. 1984;18:1501–7.
44. Ho YS, McKay G. Pseudo-second order model for sorption processes. Process Biochem. 1999 Jul;34(5):451–65.
45. Cope FW. Generalizations of the Roginsky-Zeldovich (or Elovich) equation for charge transport across biological surfaces. Bull Math Biophys. 1972 Sep 1;34(3):419–27.
46. Marczewski AW. Application of mixed order rate equations to adsorption of methylene blue on mesoporous carbons. Appl Surf Sci. 2010;256(17):5145–52.
47. Hu Q, Pang S, Wang D. In-depth Insights into Mathematical Characteristics, Selection Criteria and Common Mistakes of Adsorption Kinetic Models: A Critical Review. Sep Purif Rev. 2021 Jul 1;0(0):1–19.
48. Haerifar M, Azizian S. Fractal-Like Kinetics for Adsorption on Heterogeneous Solid Surfaces. J Phys Chem C. 2014 Jan 6;118:1129–34.
49. Tseng RL, Wu PH, Wu FC, Juang RS. A convenient method to determine kinetic parameters of adsorption processes by nonlinear regression of pseudo-nth-order equation. Chem Eng J. 2014 Feb 1;237:153–61.
50. Weng CH, Pan YF. Adsorption characteristics of methylene blue from aqueous solution by sludge ash. Colloids Surf Physicochem Eng Asp. 2006 Feb 15;274(1):154–62.
51. Kuo S, Lotse E. Kinetics of phosphate adsorption and desorption by hematite and gibbsite1. Soil Sci. 1973 Dec 1;116:400–6.
52. Avrami M. Kinetics of Phase Change. II Transformation-Time Relations for Random Distribution of Nuclei. J Chem Phys. 1940 Feb 1;8:212–24.
53. Haerifar M, Azizian S. An exponential kinetic model for adsorption at solid/solution interface. Chem Eng J. 2013 Jan 15;s 215–216:65–71.
54. Wilczak A, Keinath T. Kinetics of sorption and desorption of copper(II) and lead(II) on activated carbon. Water Environ Res. 1993 May 1;65:238–44.
55. Eris S, Azizian S. Analysis of adsorption kinetics at solid/solution interface using a hyperbolic tangent model. J Mol Liq. 2017 Feb 1;231.
56. Brouers F, Al-Musawi TJ. Brouers-Sotolongo fractal kinetics versus fractional derivative kinetics: A new strategy to analyze the pollutants sorption kinetics in porous materials. J Hazard Mater. 2018 May 15;350:162–8.
57. Brouers F, Sotolongo-Costa O. Generalized fractal kinetics in complex systems (application to biophysics and biotechnology). Phys Stat Mech Its Appl. 2006;368(1):165–75.
58. Nayak AK, Pal A. Development and validation of an adsorption kinetic model at solid-liquid interface using normalized Gudermannian function. J Mol Liq. 2019 Feb 15;276:67–77.
59. Lawal WA, Choi H. Feasibility Study on the Removal of Perfluorooctanoic Acid by Using Palladium-Doped Nanoscale Zerovalent Iron. J Environ Eng. 2018 Nov 1;144(11):04018115.
60. Wayman M, Tseng MC. Inhibition-threshold substrate concentrations. Biotechnol Bioeng. 1976;18(3):383–7.
61. Głuszcz P, Petera J, Ledakowicz S. Mathematical modeling of the integrated process of mercury bioremediation in the industrial bioreactor. Bioprocess Biosyst Eng. 2011;34(3):275–85.
62. Kass RE, Raftery AE. Bayes Factors. J Am Stat Assoc. 1995 Jun 1;90(430):773–95.
63. Burnham KP, Anderson DR. Model Selection and Multimodel Inference: A Practical Information-Theoretic Approach. Springer Science & Business Media; 2002. 528 p.
64. Foo KY, Hameed BH. Textural porosity, surface chemistry and adsorptive properties of durian shell derived activated carbon prepared by microwave assisted NaOH activation. Chem Eng J. 2012 Apr;187:53–62.
65. Kebir M, Trari M, Maachi R, Nasrallah N, Amrane A. Valorization of Inula viscosa waste extraction, modeling of isotherm, and kinetic for the tartrazine dye adsorption. Desalination Water Treat. 2015 Jun 1;54.
66. Chukwuemeka-Okorie HO, Ekuma FK, Akpomie KG, Nnaji JC, Okereafor AG. Adsorption of tartrazine and sunset yellow anionic dyes onto activated carbon derived from cassava sievate biomass. Appl Water Sci. 2021;11(2).
67. Gautam PK, Shivapriya PM, Banerjee S, Sahoo AK, Samanta SK. Biogenic fabrication of iron nanoadsorbents from mixed waste biomass for aqueous phase removal of alizarin red S and tartrazine: Kinetics, isotherm, and thermodynamic investigation. Environ Prog Sustain Energy. 2020;39(2).
68. Goscianska J, Ciesielczyk F. Lanthanum enriched aminosilane-grafted mesoporous carbon material for efficient adsorption of tartrazine azo dye. Microporous Mesoporous Mater. 2019;280:7–19.
69. Mirzajani R, Karimi S. Ultrasonic assisted synthesis of magnetic Ni-Ag bimetallic nanoparticles supported on reduced graphene oxide for sonochemical simultaneous removal of sunset yellow and tartrazine dyes by response surface optimization: Application of derivative spectrophotometry. Ultrason Sonochem. 2019;50:239–50.
70. Torres-Pérez J, Muñoz-Armenta G, Réyes-López SY. Effect of microwave treatment onto activated carbon produced from pecan nut shells for Tartrazine removal from aqueous media. Int J Environ Pollut. 2018;63(4):298–319.
71. Albadarin AB, Charara M, Abu Tarboush BJ, Ahmad MNM, Kurniawan TA, Naushad M, et al. Mechanism analysis of tartrazine biosorption onto masau stones; a low cost by-product from semi-arid regions. J Mol Liq. 2017;242:478–83.
72. Gautam RK, Banerjee S, Sanroman MA, Chattopadhyaya MC. Synthesis of copper coordinated dithiooxamide metal organic framework and its performance assessment in the adsorptive removal of tartrazine from water. J Environ Chem Eng. 2017;5(1):328–40.
73. Bacioiu IG, Stoica L, Constantin C, Stanescu AM. Adsorption equilibrium and kinetics modeling for tartrazine(E102) – Fe(II) based adsorbent system. Rev Chim. 2016;67(12):2391–5.
74. Alcántara-Cobos A, Solache-Ríos MJ, Díaz-Nava MDC. Adsorption of tartrazine on an iron modified zeolitic tuff. Environ Eng Manag J. 2016;15(11):2453–8.
75. Gautam PK, Gautam RK, Banerjee S, Lofrano G, Sanroman MA, Chattopadhyaya MC, et al. Preparation of activated carbon from Alligator weed (Alternenthera philoxeroids) and its application for tartrazine removal: Isotherm, kinetics and spectroscopic analysis. J Environ Chem Eng. 2015;3(4):2560–8.
76. Ansari R, Keivani MB, Delavar AF. Application of polyaniline nanolayer composite for removal of tartrazine dye from aqueous solutions. J Polym Res. 2011;18(6):1931–9.
77. Rodríguez-Zapién KV, Torres-Pérez J, Reyes-López SY. Environmental application of quartz-based construction waste: tartrazine removal from aqueous media. Int J Environ Sci Technol. 2022;19(10):10381–92.
78. Balayeva OO, Azizov AA, Muradov MB, Alosmanov RM. Removal of tartrazine, ponceau 4R and patent blue V hazardous food dyes from aqueous solutions with ZnAl-LDH/PVA nanocomposite. J Dispers Sci Technol. 2021;
79. Foo KY, Hameed BH. Insights into the modeling of adsorption isotherm systems. Chem Eng J. 2010;156(1):2–10.
80. Yaneva ZL, Georgieva NV. Insights into Congo Red adsorption on agro-industrial materials - spectral. Int Rev Chem Eng. 2012;4(2):127–46.

81. Azizian S. Kinetic models of sorption: A theoretical analysis. J Colloid Interface Sci. 2004;276(1):47–52.
82. Tykodi R. Kinetics and thermodynamics of adsorption of dyes on activated carbon fibers. J Environ Manage. 2004;71(4):305–15.
83. Lin J, Wang Y. Kinetics of adsorption of dyes from aqueous solution onto modified corn straw. J Hazard Mater. 2009;161(2–3):923–8.
84. Simonin O. Kinetics and thermodynamics of adsorption of dyes on activated carbon fibers. J Environ Manage. 2016;181:100–9.
85. Hu Y, Li L, Wang Y. Kinetics of adsorption of anionic and cationic dyes on biochar. J Environ Manage. 2018;212:166–74.
86. Moussout N, Simonin O, Leclère Q. Kinetics and thermodynamics of adsorption of anionic and cationic dyes on biochars. J Environ Manage. 2018;210:112–20.
87. Ho YS, McKay G, Healy TW. The intraparticle diffusion model applied to adsorption systems. J Colloid Interface Sci. 2000;230(2):117–25.
88. Plazinski J, Rudzinski W. Kinetics of adsorption of dyes from aqueous solutions on activated carbon. J Colloid Interface Sci. 2009;335(2):476–81.
89. Gautam RK, Gautam PK, Banerjee S, Rawat V, Soni S, Sharma SK, et al. Removal of tartrazine by activated carbon biosorbents of *Lantana camara*: Kinetics, equilibrium modeling and spectroscopic analysis. J Environ Chem Eng. 2015;3(1):79–88.
90. Wan Ngah WS, Ariff NFM, Hanafiah MAKM. Preparation, Characterization, and Environmental Application of Crosslinked Chitosan-Coated Bentonite for Tartrazine Adsorption from Aqueous Solutions. Water Air Soil Pollut. 2010 Feb 1;206(1):225–36.
91. Mittal A, Mittal J, Kurup L. Adsorption isotherms, kinetics and column operations for the removal of hazardous dye, Tartrazine from aqueous solutions using waste materials—Bottom Ash and De-Oiled Soya, as adsorbents. J Hazard Mater. 2006 Aug 25;136(3):567–78.
92. Dotto GL, Vieira MLG, Pinto LAA. Kinetics and Mechanism of Tartrazine Adsorption onto Chitin and Chitosan. Ind Eng Chem Res. 2012 May 16;51(19):6862–8.